

## Modular and Versatile Hybrid Coordination Motifs on $\alpha$ -Helical Protein Surfaces

Robert J. Radford, Phuong C. Nguyen, and F. Akif Tezcan\*

Department of Chemistry and Biochemistry, University of California, San Diego,  
9500 Gilman Dr., La Jolla, California 92093-0356

Received May 9, 2010

We report here the construction of phenanthroline (Phen) and terpyridine (Terpy)-based hybrid coordination motifs (HCMs), which were installed on the surface of the four-helical bundle heme protein cytochrome *cb*<sub>562</sub>. The resulting constructs, termed HPhen1, HPhen2, HPhen3, and HTerpy1, feature HCMs that are composed of a histidine ligand and a Phen or Terpy functionality located two helix turns away, yielding stable tri- or tetradentate coordination platforms. Our characterization of the tridentate HCMs indicates that they accommodate many divalent metal ions (Co<sup>2+</sup>, Ni<sup>2+</sup>, Cu<sup>2+</sup>, Zn<sup>2+</sup>) with nanomolar to femtomolar affinities, lead to significant stabilization of the  $\alpha$ -helical protein scaffold through metal-mediated cross-linking, assert tight control over protein dimerization, and provide stable and high-affinity binding sites for substitution-inert metal probes. Our analyses suggest that such tridentate HCMs may be used modularly on any  $\alpha$ -helical protein surface in a sequence-independent fashion.

### Introduction

The primary biological roles of metals including catalysis, electron transfer, and structural stabilization are generally established once they are firmly placed within a protein scaffold.<sup>1</sup> Owing to the stability of the resulting complexes, the interactions between metals and the interiors of proteins are readily characterized and have justifiably formed the focus of bioinorganic chemistry. One could argue, on the other hand, that metals spend a good majority of their time interacting with protein surfaces and that such transient, harder-to-characterize interactions carry in vivo and in vitro consequences that rival those of metal–protein interior interactions. The prevalence of metal–protein surface interactions becomes especially clear when picturing the behavior of metal ions and complexes within the crowded cellular environment, for example, as they are being passed on from one specific protein (e.g., a metallochaperone)<sup>2</sup> to another, or as they cross-link together multiple proteins whose aggregation may have dire consequences.<sup>3</sup> Similarly, outside the cellular realm, metal–protein surface interactions form the basis of immobilized metal ion affinity chromatography (IMAC)<sup>4</sup> as well as the functionalization of protein surfaces with metal complexes that have

served as invaluable spectroscopic and functional probes.<sup>5,6</sup> Given such broad importance and utility of metal–protein surface interactions, we envisioned a need for metal coordinating motifs that would enable a better control of inorganic chemistry on protein surfaces.

Our original interest in metal–protein surface interactions stems from our desire to use metal coordination chemistry to direct protein–protein interactions (PPIs)<sup>7</sup> and protein self-assembly more predictably and readily than computational design approaches. One caveat to utilizing metal coordination to control PPIs is the presence of numerous metal-binding side-chain functionalities on any given protein surface, which bring about the challenge of controlling metal localization. In one strategy to circumvent this challenge, we introduced a Cys-specific bidentate non-natural chelate (5-iodoacetamido-1,10 phenanthroline, IA-Phen) onto the surface of a four-helix-bundle protein, cytochrome *cb*<sub>562</sub>, which led to the Ni<sup>2+</sup>-driven formation of an unusual triangular protein architecture.<sup>8</sup> More recently, to exert more control over metal localization as well as metal-directed protein self-assembly, we used another bidentate chelate (5-iodoacetamido-8-hydroxyquinoline, IA-Quin) attached to a Cys (C70) in combination with a His (H63) located two helix turns away on the cyt *cb*<sub>562</sub> surface, yielding the construct HQuin1 (Figure 1a).<sup>9</sup> The resulting

\*To whom correspondence should be addressed. E-mail: tezcan@ucsd.edu.  
(1) Bertini, I.; Gray, H. B.; Stiefel, E. I.; Valentine, J. S. *Biological Inorganic Chemistry, Structure & Reactivity*; University Science Books: Sausalito, CA, 2007.  
(2) Rosenzweig, A. C. *Acc. Chem. Res.* 2001, 34, 119–128.  
(3) Bush, A. I.; Pettingell, W. H.; Multhaupt, G.; Paradis, M. D.; Vonsattel, J. P.; Gusella, J. F.; Beyreuther, K.; Masters, C. L.; Tanzi, R. E. *Science* 1994, 265, 1464–1467.  
(4) Arnold, F. H.; Haymore, B. L. *Science* 1991, 252, 1796–1797.  
(5) Winkler, J. R.; Gray, H. B. *Chem. Rev.* 1992, 92, 369–379.  
(6) Adams, S. R.; Campbell, R. E.; Gross, L. A.; Martin, B. R.; Walkup, G. K.; Yao, Y.; Llopis, J.; Tsien, R. Y. *J. Am. Chem. Soc.* 2002, 124, 6063–6076.

(7) (a) Salgado, E. N.; Faraone-Mennella, J.; Tezcan, F. A. *J. Am. Chem. Soc.* 2007, 129, 13374–13375. (b) Salgado, E. N.; Lewis, R. A.; Faraone-Mennella, J.; Tezcan, F. A. *J. Am. Chem. Soc.* 2008, 130, 6082–6084. (c) Salgado, E. N.; Lewis, R. A.; Mossin, S.; Rheingold, A. L.; Tezcan, F. A. *Inorg. Chem.* 2009, 48, 2726–2728.  
(8) Radford, R. J.; Tezcan, F. A. *J. Am. Chem. Soc.* 2009, 131, 9136–9137.  
(9) Radford, R. J.; Nguyen, P. C.; Ditri, T. B.; Figueroa, J. S.; Tezcan, F. A. *Inorg. Chem.* 2010, 49, 4362–4369.  
(10) Martell, A. E.; Smith, R. M. *Critical Stability Constants*; Plenum Press: New York, 1974.

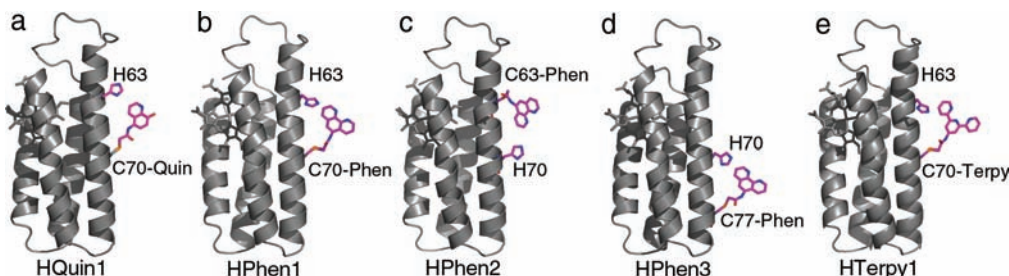


**Figure 1.** Cartoon representations for various HCM-bearing *cyt cb*<sub>562</sub> variants. Functionalities that comprise the HCMs and the heme groups are shown as sticks.

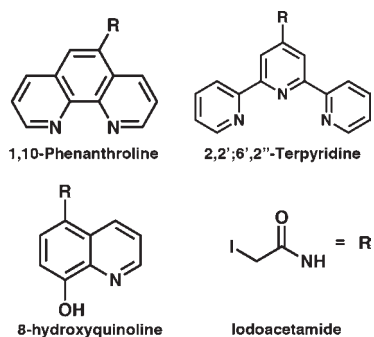


**Figure 2.** Phenanthroline (Phen), terpyridine (Terpy), and hydroxyquinoline (Quin) derivatives used for the construction of HCMs in this study. The iodoacetamide moiety is attached to the chelating functionalities through the amide nitrogen.

*i/i+7* hybrid coordination motif (HCM) was shown to coordinate various divalent metal ions in a tridentate fashion, which led to (1) high affinity divalent metal binding with dissociation constants ( $K_d$ 's) ranging from nanomolar to femtomolar, (2) stabilization of the protein scaffold via metal-mediated cross-linking of a two-helix turn segment, and (3) tight control over protein dimerization via an octahedral metal coordination geometry. Several potential applications could arise from these advantages, including site-selective labeling of proteins with metal probes, improved protein separation with IMAC, stabilization of small helical peptides for pharmaceutical purposes, and manipulation of cellular pathways that depend on protein dimerization.

Given such possibilities and the ease of constructing an HCM via iodoacetamide (IA)–Cys coupling, we have sought to examine in the present study whether the advantageous properties of the HQuin1 HCM are generalizable, i.e., whether the *i/i+7* HCMs that consist of a His and a non-natural chelating ligand can be utilized in a modular fashion on any  $\alpha$ -helical surface. Toward this end, we have created a series of additional *cyt cb*<sub>562</sub>-based constructs (Figure 1b–e), which have been functionalized with various non-natural chelates (Figure 2): (a) HPhen1, the phenanthroline (Phen)-derivatized counterpart of HQuin1, was constructed to probe the generality of the non-natural component. (b) HPhen2, which features the opposite placement of His and the Cys–Phen group of that in HPhen1 (Cys63 in the *i* and His70 in the *i+7* position), was constructed to test the sensitivity of the *i/i+7* HCM to the relative placement of the natural and non-natural ligands. (c) HPhen3, which has the HCM motif located elsewhere on the *cyt cb*<sub>562</sub> surface (His70, Cys77), was generated to test the sensitivity of the HCM to location,

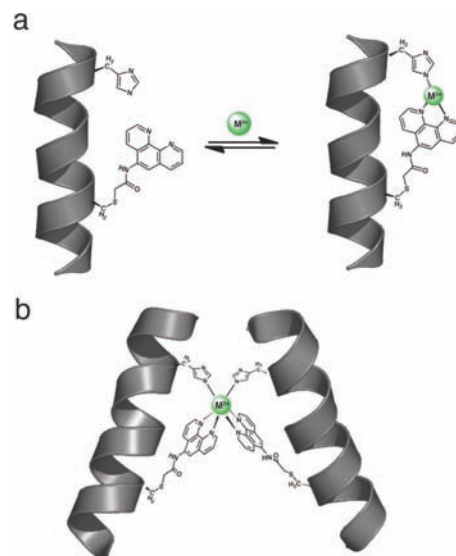


**Figure 3.** (a) Three-coordinate, facial metal binding to a His–Phen HCM. (b) Proposed mode of metal-dependent dimerization mediated by a *i/i+7* His–Phen HCM.

and (d) HTerpy1, the terpyridine-derivatized counterpart of HQuin1, was generated to feature a tetradentate HCM. We present here the characterization of these constructs in terms of their metal binding affinities, metal-dependent stabilization, and metal-dependent oligomerization properties (Figure 3). Our results suggest that the *i/i+7* HCMs may be modularly utilized on any  $\alpha$ -helical protein surface toward a number of applications.

## Results and Discussion

**Construction of *cyt cb*<sub>562</sub> Variants with Quin-, Phen-, and Terpy-Bearing HCMs.** A requisite for expanding the biological and chemical utility of HCMs is to demonstrate the modularity of the non-natural metal chelator and the ease of its incorporation. To this end, we site-specifically labeled *cyt cb*<sub>562</sub> variants bearing a single surface Cys residue with IA-derivatized versions of the ubiquitous metal chelators Phen, Terpy, and Quin to create the HCM variants shown in Figure 1. These non-natural ligands were chosen because they are commercially available as—or easily converted to—amino-functionalized precursors, their coordination chemistry has been extensively studied, and they represent a small but diverse set of ligands with variations in denticity and overall charge.

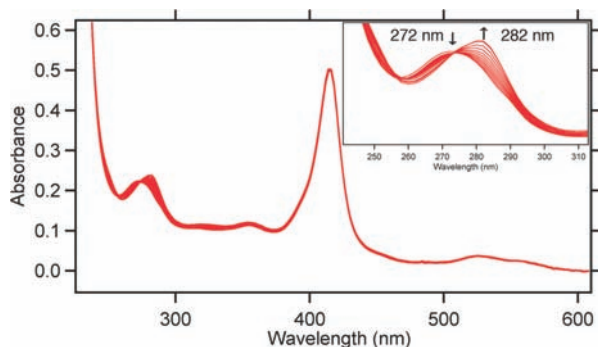


**Figure 4.** Spectral changes that accompany  $\text{Zn}^{2+}$  binding to HPhen1 as monitored by UV-vis spectroscopy. Spectra show a typical ferric heme spectrum with a Soret band at 415 nm ( $\epsilon = 0.148 \mu\text{M}^{-1} \text{cm}^{-1}$ ) along with a transition between metal-free ( $\lambda_{\text{max}} = 272 \text{ nm}$ ) and metal-bound ( $\lambda_{\text{max}} = 282 \text{ nm}$ ) Phen species. Inset: Close-up view of the UV region showing a clean isosbestic point at 274 nm consistent with a 1:1  $\text{Zn}^{2+}$ /Phen binding model.

The amino precursors of Phen, Quin, and Terpy were converted in a one-pot reaction with iodoacetic anhydride or iodoacetyl chloride into IA derivatives with 60–75% yield. Although IA-Phen, IA-Quin, and IA-Terpy are sparingly soluble in water, they are easily introduced into cyt *cb*<sub>562</sub> solutions after being solubilized in DMF or DMSO; we have found no adverse effects of these organic solvents on cyt *cb*<sub>562</sub> up to a final volume fraction of 50% versus  $\text{H}_2\text{O}$ . Cys functionalization reactions proceed rapidly and specifically (provided that the solution pH is kept below 8 to prevent Lys labeling), with overall yields of modification ranging from 60% for IA-Terpy to 95% for IA-Phen after purification. In the case of cyt *cb*<sub>562</sub>, the functionalized products are readily separated from non-functionalized protein using ion-exchange chromatography (Figure S1.1, Supporting Information).

**Metal Binding Properties of Phen- and Terpy-Based HCMs.** We had previously examined the divalent metal-binding properties of HQuin1 and confirmed that the *i/i+7* His–Quin HCM was able to coordinate metals in a facial, tridentate geometry.<sup>9</sup> Here, we have performed similar metal-binding titrations for HPhen1, HPhen2, and HPhen3 using late first-row transition metals ( $\text{Co}^{2+}$ ,  $\text{Ni}^{2+}$ ,  $\text{Cu}^{2+}$ , and  $\text{Zn}^{2+}$ ) to probe whether the Phen functionality behaves similarly to Quin in the context of an HCM. It is important to note that the relative positions of the coordinating atoms to the point of protein attachment in the Phen derivative are equivalent to those in the Quin derivative (Figure 2). Metal binding by the His–Phen HCMs was monitored by the distinct 10-nm red-shift in the  $\pi$ – $\pi^*$  absorption band for Phen (metal-free  $\lambda_{\text{max}} = 272 \text{ nm}$ ; metal-bound  $\lambda_{\text{max}} = 282 \text{ nm}$ ) upon metal binding (Figure 4). It was confirmed through CD spectroscopy that the  $\alpha$ -helical fold is not significantly perturbed by metal binding to the HCMs (Figure S1.19, Supporting Information).

As in the case of HQuin1, it was quickly established that Phen-based HCMs bind all tested divalent metals very tightly, which required all titrations to be performed in the presence of ethylene glycol tetraacetic acid (EGTA) as a competing ligand. Due to the inherent ability of Phen-based HCMs to undergo metal-mediated dimerization (Figure 3b), protein concentrations were kept sufficiently low ( $<5 \mu\text{M}$ ) to minimize dimer formation. In all cases (HPhen1–3 and

all metals), the metal binding isotherms were satisfactorily described by a 1:1 binding model (Figures 5 and S1.2 and S1.3, Supporting Information).

An analysis of the determined dissociation constants (Table 1) reveals that all Phen-based HCMs display a significant increase in affinity over free Phen for the late first row transition metals, which strongly suggests the participation of the His component of the HCMs in metal binding. Moreover, the affinities of HPhen1, -2, and -3 for divalent metals are similar and vary at most by 6-fold, indicating that metal binding ability is not very sensitive to helix location or relative orientation of the HCM (see below for a discussion on the possible effects of intervening residues).

In addition to the HPhen variants, we investigated whether HTerpy1 (Figure 1e) can engage both Terpy and His in a tetradentate coordination motif. Metal binding titrations and sedimentation velocity (SV) experiments reveal that HTerpy1 almost exclusively forms a stable dimer with a saturation point reached upon the addition of half of an equivalent of  $\text{M}^{2+}$  (Figure S1.4, Supporting Information), which has precluded the determination of the HTerpy1 metal binding affinities. While protein unfolding studies (see below) show evidence for metal coordination by both His and Terpy, the unstrained, facial coordination geometry observed in HQuin1 and HPhen variants cannot be accommodated by the large Terpy group, leading to the formation of the thermodynamically and kinetically stable *bis*-Terpy adduct involving two proteins.

**Metal-Mediated Protein Stabilization through Phen- and Terpy-Based HCMs.** We next sought to determine if the Phen- and Terpy-based HCMs would have any stabilizing effect on the protein scaffold. Since HCMs cross-link a  $\sim 7$ -Å long, two-helix-turn segment of cyt *cb*<sub>562</sub> through metal coordination, an increase in the global stability of the protein should be expected. Metal cross-linking of both natural and non-natural residues at *i/i+4* positions has extensively been shown to induce  $\alpha$ -helicity in peptides and significantly stabilize helical protein structures.<sup>11,12</sup> Likewise, covalent cross-linking of side chain functionalities in *i/i+4*, *i/i+7*, or *i/i+11* positions can lock small peptides in  $\alpha$ -helical conformations,<sup>13–15</sup> which in turn have proven to be promising pharmaceutical agents that effectively disrupt protein–protein interactions and exhibit increased resistance to proteases *in vivo*.<sup>16</sup>

In order to investigate the cross-linking ability of HCMs in the presence of metals, chemical and thermal unfolding studies were undertaken. In a typical chemical unfolding experiment, a solution of folded HPhen or HTerpy variant was titrated with increasing amounts of unfolded protein solution prepared in 8 M guanidine hydrochloride (GuHCl).

(11) Ghadiri, M. R.; Choi, C. *J. Am. Chem. Soc.* **1990**, *112*, 1630–1632.

(12) Ruan, F. Q.; Chen, Y. Q.; Hopkins, P. B. *J. Am. Chem. Soc.* **1990**, *112*, 9403–9404.

(13) Blackwell, H. E.; Grubbs, R. H. *Angew. Chem., Int. Ed.* **1998**, *37*, 3281–3284.

(14) Schafmeister, C. E.; Po, J.; Verdine, G. L. *J. Am. Chem. Soc.* **2000**, *122*, 5891–5892.

(15) Zhang, F. Z.; Sadowski, O.; Xin, S. J.; Woolley, G. A. *J. Am. Chem. Soc.* **2007**, *129*, 14154–14155.

(16) Verdine, G. L.; Walensky, L. D. *Clin. Cancer Res.* **2007**, *13*, 7264–7270.

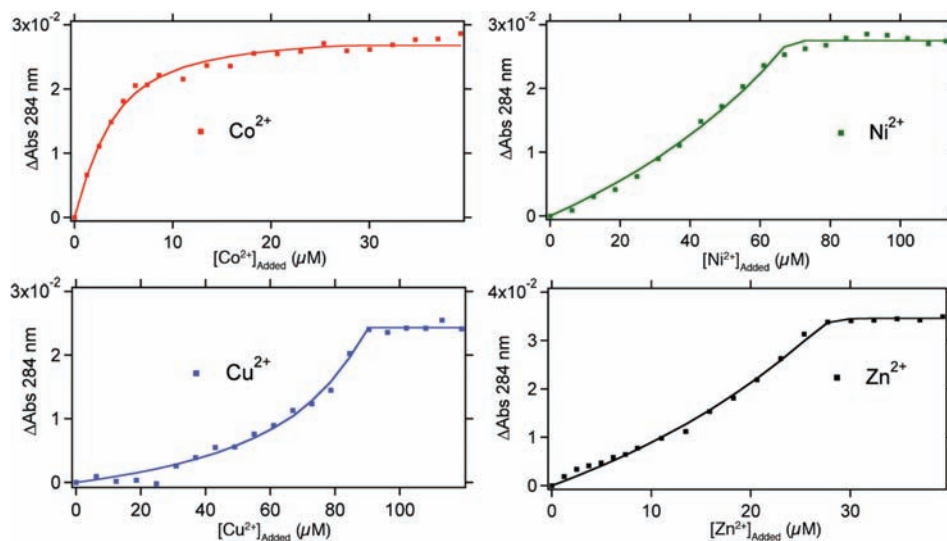


**Figure 5.** Metal-binding titration data and fits for HPhen1 as monitored by UV–visible spectroscopy. A typical titration sample contained 2–5  $\mu\text{M}$  HPhen1, 50 mM MOPS (pH 7), and 20–100  $\mu\text{M}$  EGTA. All data were described satisfactorily by a 1:1 binding model. Binding isotherms for HPhen2 and HPhen3 are shown in Figures S1.2 and S1.3 (Supporting Information). Dissociation constants ( $K_d$ ) determined are listed in Tables 1 and S2.1 (Supporting Information).

**Table 1.** Dissociation Constants for HPhen–Metal Complexes Compared to Those for Free 1,10-Phenanthroline (Phen)

|                  | dissociation constants (M) |                          |                          |                        |
|------------------|----------------------------|--------------------------|--------------------------|------------------------|
|                  | HPhen1 <sup>a</sup>        | HPhen2 <sup>a</sup>      | HPhen3 <sup>a</sup>      | free Phen <sup>b</sup> |
| Co <sup>2+</sup> | $3.3(2) \times 10^{-10}$   | $7.8(5) \times 10^{-10}$ | $2.0(2) \times 10^{-9}$  | $8.0 \times 10^{-8}$   |
| Ni <sup>2+</sup> | $7.8(6) \times 10^{-10}$   | $1.7(4) \times 10^{-10}$ | $1.6(3) \times 10^{-10}$ | $3.9 \times 10^{-8}$   |
| Cu <sup>2+</sup> | $1.3(2) \times 10^{-13}$   | $1.2(2) \times 10^{-13}$ | $2.0(2) \times 10^{-13}$ | $2.5 \times 10^{-9}$   |
| Zn <sup>2+</sup> | $6(1) \times 10^{-9}$      | $3.8(3) \times 10^{-9}$  | $3.7(3) \times 10^{-8}$  | $3.9 \times 10^{-7}$   |

<sup>a</sup> Dissociation constants determined by competition with EGTA in 50 mM MOPS (pH 7). <sup>b</sup> pH-adjusted values based on reported  $K_d$ 's.<sup>10</sup>

The folding/unfolding transition was followed by CD spectroscopy, monitoring changes in ellipticity at 222 nm. Thermal unfolding measurements spanning 298 to 373 K were similarly monitored at 222 nm; because of the high stability of all variants, 1.5 M GuHCl was included in each sample to ensure that complete unfolding took place before 373 K. In both chemical and thermal unfolding experiments, metals were present in large excess over protein to ensure full occupancy of HCMs, thereby preventing metal-induced dimerization.

The stability of all HPhen and HTerpy variants tested was found to increase in the presence of divalent metal ions. Figure 6 shows representative unfolding titrations of the variants, each of which display a particularly enhanced stability in the presence of Ni<sup>2+</sup> (for other metals and thermal titrations, see Figures S1.5–9, Supporting Information); a complete set of results is given in Table 2. At least in the case of the HPhen variants, we attribute the superior stabilizing effect of Ni<sup>2+</sup> over other metals to the formation of an unstrained, facial coordination geometry by the His–Phen HCM, which was previously shown to be the case for the His–Quin HCM.

In order to establish that the observed protein stabilization is due to metal-mediated, intrahelical cross-linking, we carried out the unfolding titrations of HPhen1 and HTerpy1 at pH 5.5, where the His component of the HCM should be partially protonated and unable to fully coordinate metals (Figures 7a and b). Additional

unfolding titrations were performed for variants of HPhen1 and HTerpy1, where either the Phen or the Terpy moiety is replaced by a carboxymethyl group (CM-G70C cyt *cb*<sub>562</sub>, Figure S1.10, Supporting Information) or the His63 residue is mutated to Ala (APhen1 and ATerpy1, Figures 7c,d and S1.11, Supporting Information). The results indicate that, in all cases, Ni-induced stabilization is significantly diminished, confirming the involvement of both His and Phen (or Terpy) in metal coordination.

It is tempting to link the thermodynamics of metal binding by the HCMs (Table 1) to that of metal-induced protein stabilization (Table 2). Nevertheless, such a correlation is complicated by the fact that net protein stabilization is a function of metal binding not only to the folded but also to the unfolded state, which may display multiple modes of metal coordination (thus deviating from a two-state system). We therefore have avoided presenting free energies of unfolding—which assumes a two-state process—for our variants in the presence of metals. A good case in point is Cu<sup>2+</sup>, which displays by far the highest affinity for any HCM yet leads to the smallest extent of stabilization (Table 2). Regardless, the protein unfolding titrations indicate that (1) all Phen-based HCMs lead to a measurable metal-induced increase in protein stability, (2) this stabilization is not specific to a particular HCM location or orientation, and, finally, (3) the Terpy–His HCM displays a diminished stabilizing effect due likely to an unfavorable metal coordination geometry.

#### Metal-Dependent Self-Assembly Properties of HPhen1.

The ability to control protein self-assembly, both temporally and spatially, is an intensely pursued goal that is complicated by the necessity to design extensive molecular surfaces.<sup>17,18</sup> Particularly challenging is directing the self-assembly of proteins into discrete shapes that can recognize

(17) Kortemme, T.; Baker, D. *Curr. Opin. Chem. Biol.* **2004**, *8*, 91–97.

(18) Shoemaker, B. A.; Panchenko, A. R. *PLoS Comput. Biol.* **2007**, *3*, 595–601.

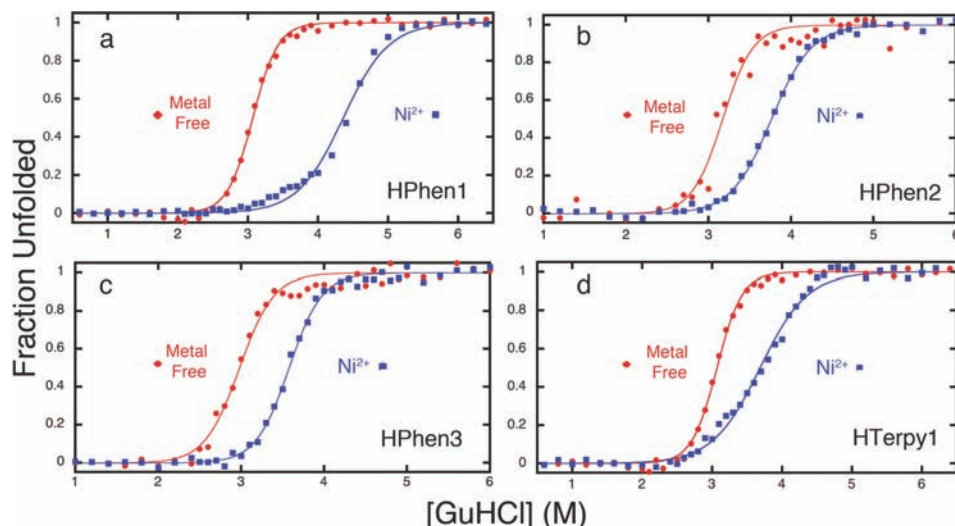


**Figure 6.** Chemical unfolding titrations of (a) HPhen1, (b) HPhen2, (c) HPhen3, and (d) HTerpy1 in the presence and absence of  $\text{Ni}^{2+}$  as monitored by CD spectroscopy at 222 nm.

**Table 2.** Observed Changes in the Midpoint for the Unfolding Transition ( $\Delta[\text{GuHCl}]_m$ ) for HPhen and HTerpy Variants upon Metal Binding

|         | $\Delta[\text{GuHCl}]_m$ (M) |                  |                  |                  |
|---------|------------------------------|------------------|------------------|------------------|
|         | $\text{Co}^{2+}$             | $\text{Ni}^{2+}$ | $\text{Cu}^{2+}$ | $\text{Zn}^{2+}$ |
| HPhen1  | 0.84                         | 1.15             | 0.41             | 0.78             |
| HPhen2  | 0.25                         | 0.6              | 0.22             | 0.4              |
| HPhen3  | 0.24                         | 0.6              | -0.02            | 0.29             |
| HTerpy1 | 0.21                         | 0.47             | 0.01             | 0.32             |
| APhen1  | 0.02                         | 0.12             | -0.19            | 0.01             |

biological targets. An exciting finding about HQuin1 was its ability to specifically dimerize upon  $\text{Ni}^{2+}$  binding into a rigid architecture that was shaped appropriately to bind major grooves of a double-helical DNA.<sup>9</sup> Since HPhen1 is the closest in composition and chemical behavior to HQuin1, which we had already structurally characterized, we chose to explore its metal-dependent self-assembly properties as a representative of all Phen-bearing variants.

Sedimentation velocity (SV) experiments reveal that HPhen1 readily dimerizes in the presence of half an equivalent of  $\text{Ni}^{2+}$  with a sedimentation coefficient of 2.6 S, similar to that of the  $\text{Ni}:\text{HQuin1}_2$  complex (Figure 8a).<sup>9</sup> The dissociation constant for the  $\text{Ni}:\text{HPhen1}_2$  dimer ( $K_{d(2\text{mer}-1\text{mer})}$ ) was determined by sedimentation equilibrium (SE) experiments to be  $\sim 9 \mu\text{M}$ , which is lower than the  $K_{d(2\text{mer}-1\text{mer})}$  of  $42 \mu\text{M}$  for  $\text{Ni}:\text{HQuin1}_2$  (Figure 8b and Figure S1.12, Supporting Information).<sup>9</sup> Significantly, the dimeric stability of  $\text{Ni}:\text{Phen1}_2$  now closely approximates that of the bZIP family of transcription factors, which use peripheral leucine zipper domains for dimerization, with  $K_d$ 's in the low micromolar range.<sup>19</sup>

Complete structural characterization of the  $\text{Ni}:\text{HPhen1}_2$  dimer has remained elusive to this point. However, we project—on the basis of the similarities between HPhen1 and HQuin1 and the fact that dimerization in both cases is entirely dictated by metal coordination—that the structure of  $\text{Ni}:\text{HPhen1}_2$  should closely resemble that of  $\text{Ni}:\text{HQuin1}_2$ . In the case of  $\text{Ni}:\text{HQuin1}_2$ , it was determined

through density functional theory (DFT) calculations that the most favored inner-sphere coordination arrangement would pose the Quin groups *cis* to one another in the  $\Delta$  configuration,<sup>20</sup> whereby the two phenolate Quin oxygens would lie *trans* to each other, which is also the crystallographically observed configuration.<sup>9</sup>

We performed similar DFT (BP86 and OLYP) calculations on  $\text{Ni}:\text{HPhen1}_2$ , where we investigated the relative energies of two possible inner-sphere arrangements for the His–Phen HCM: one that presents Phen ligands *cis* to one another (*cis*-Phen) and one that presents Phen ligands in a *trans* configuration (*trans*-Phen) (Figure 9). These calculations suggest that the *cis*-Phen arrangement is  $\sim 5.2$  kcal/mol more stable than the *trans*-Phen arrangement. In the case of  $\text{Ni}:\text{HQuin1}_2$ , the higher stability of the *cis*-Quin isomer was attributed to the *trans*-directing effect of the imine ligands, which would render a mutual *trans* orientation of the weaker-field phenolate ligands the least destabilized configuration. With the N,O groups of Quin now replaced with the N,N groups in the Phen ligands, this argument cannot be made to explain the higher stability of the *cis*-Phen arrangement. Instead, a close inspection of the calculated structures reveals that in the *trans*-Phen arrangement, there would be steric clashes between the Phen hydrogens that lie on the Ni equatorial plane, which would be relieved in the *cis*-Phen arrangement.

Taking together the DFT results and solution studies, we conclude that the *i/i+7* His–Phen HCM would yield a  $\text{Ni}^{2+}$ -induced V-shaped dimer that is equivalent to the crystallographically characterized  $\text{Ni}:\text{HQuin1}_2$  architecture (Figure 10).<sup>9</sup> Although the reason for the specific formation of this V-shaped structure is different for His–Quin and His–Phen HCMs, both examples demonstrate that self-assembly of the proteins can be programmed through a simple consideration of inner-sphere metal coordination, which is far more facile than designing extensive protein interfaces to the same end.

(19) Kohler, J. J.; Metallo, S. J.; Schneider, T. L.; Schepartz, A. *Proc. Natl. Acad. Sci. U.S.A.* **1999**, *96*, 11735–11739.

(20) Due to the inherent chirality of the  $\alpha$ -helical scaffolds, the  $\Delta$  configuration is not possible.

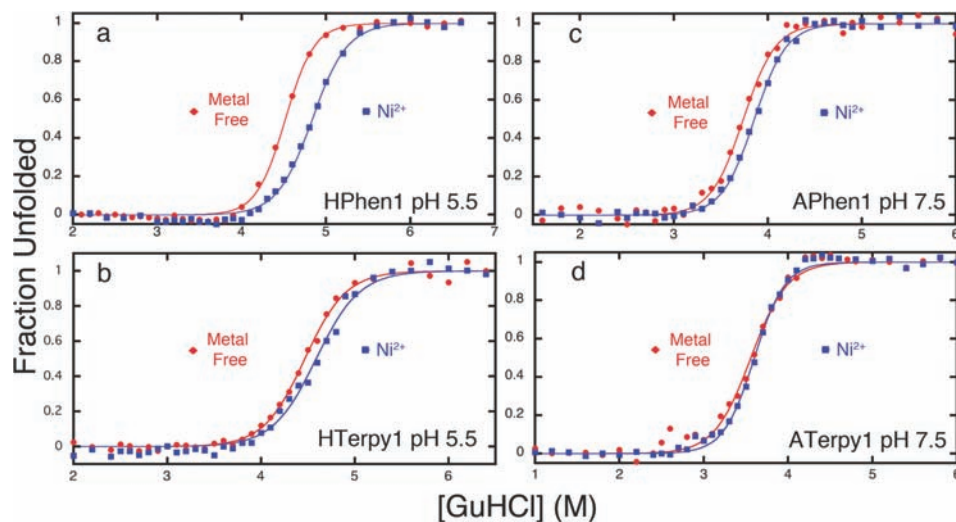


**Figure 7.** Chemical unfolding titrations of (a) HPhen1 at pH 5.5, (b) HTerpy1 at pH 5.5, (c) APhen1 at pH 7.5, and (d) HTerpy1 at pH 7.5. The lack of significant protein stabilization in the presence of  $\text{Ni}^{2+}$  ions indicates that both His and Phen or Terpy moieties are involved in metal-mediated protein cross-linking.

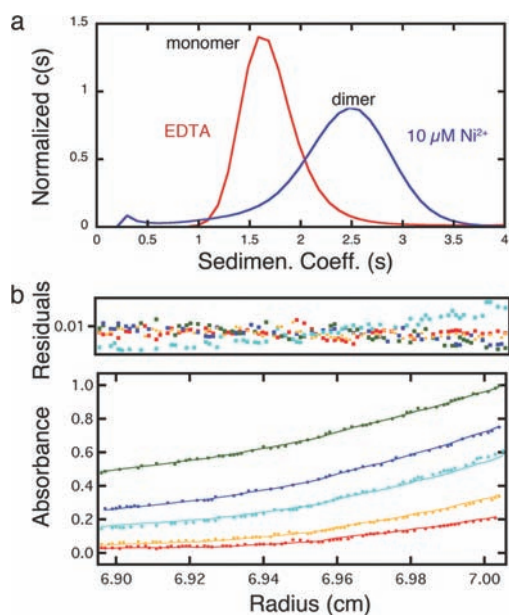


**Figure 8.** (a) Sedimentation velocity profiles of  $20\ \mu\text{M}$  HPhen1 in the absence and presence of  $\text{Ni}^{2+}$ . (b) Sedimentation equilibrium (SE) profiles for  $20\ \mu\text{M}$  HPhen1 in the presence of  $10\ \mu\text{M}$   $\text{Ni}^{2+}$ , with equilibrium speeds of 20 000 (green), 25 000 (blue), 30 000 (cyan), 35 000 (yellow), and 41 000 rpm (red). Data were fit to a monomer–dimer self-association model with a  $K_d$  of  $8.9\ (1)\ \mu\text{M}$ .

#### Using Phen-Bearing HCMs for Protein Functionalization.

Metal complexes site-specifically attached to protein surfaces have proven to be invaluable functional reporters. Among these, Ru-, Os-, and Re-polypyridyl derivatives have been widely used due to their photophysical and photochemical properties.<sup>21,22</sup> Similarly, bifunctional, As-based fluorescent reporters have been designed to specifically bind bis-Cys patterns on proteins and are finding increasing use as target-selective *in vivo* reporters.<sup>6</sup> Given the high affinity of Phen-based HCMs for divalent

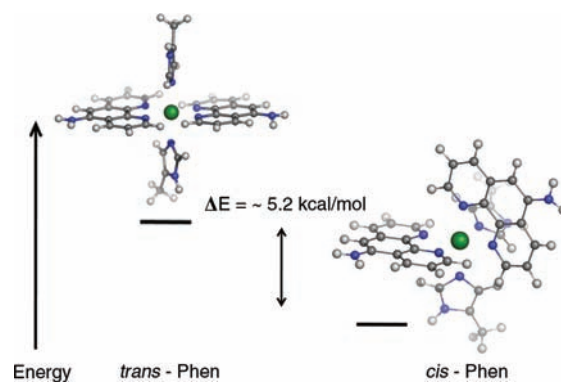


**Figure 9.** Energy minimized structures (BP86) for the proposed inner-sphere coordination geometry of the  $\text{Ni}:\text{HPhen1}_2$  dimer.

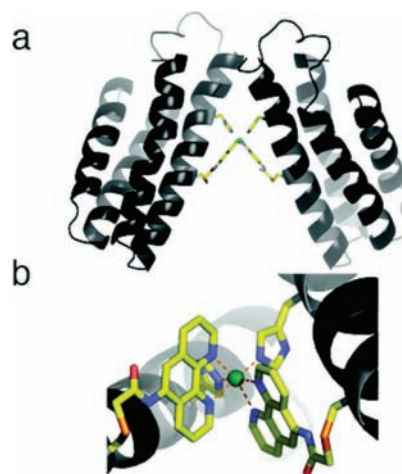


**Figure 10.** (a) The proposed  $\text{Ni}:\text{HPhen1}_2$  architecture modeled after the crystallographically determined  $\text{Ni}:\text{HQuin1}_2$  structure. (b) The corresponding inner coordination sphere.

metals and their two-point attachment to the protein scaffold, we envisioned that they could provide stable and specific target sites for functional metal-based probes on  $\alpha$ -helical proteins. Moreover, we surmised that if such probes are based on substitution-inert metals, they could

(21) Crane, B. R.; Di Bilio, A. J.; Winkler, J. R.; Gray, H. B. *J. Am. Chem. Soc.* **2001**, *123*, 11623–11631.

(22) Castellano, F. N.; Dattelbaum, J. D.; Lakowicz, J. R. *Anal. Biochem.* **1998**, *255*, 165–170.

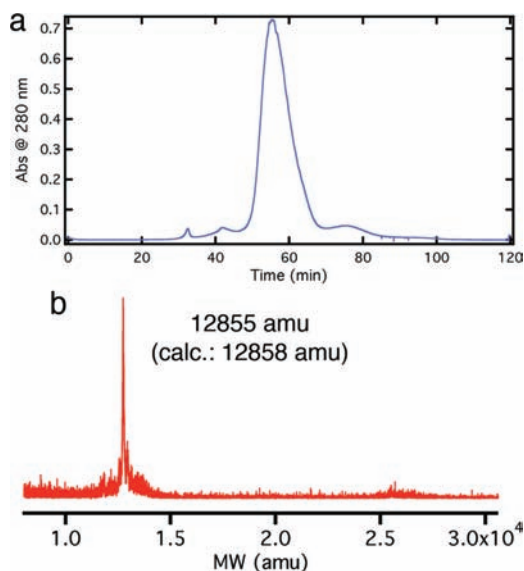
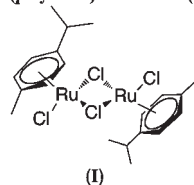


**Figure 11.** (a) Anion-exchange FPLC chromatogram of the crude Ru(*p*-cymene)–HPhen1 reaction mixture. Product eluted at 0.2–0.25 M NaCl using a linear NaCl gradient (0–0.5 M in 10 mM sodium phosphate, pH 8.0). (b) MALDI mass spectra of the major FPLC product identified as the Ru(*p*-cymene)–HPhen1 complex.

result in the improved and irreversible stabilization of  $\alpha$ -helical proteins/peptides and may be of value in terms of constructing helical peptide-based pharmaceutical agents. To investigate such possibilities, we explored the interactions of HPhen1 with a *p*-cymene-capped Ru(II) compound. We chose this particular piano-stool complex as a test case, because the Ru center is capped with an arene group (*p*-cymene), which should prevent protein dimerization and accommodate facial binding by the His–Phen HCMs. Additionally, it is commercially available in a dimeric, chloro-substituted form (**1**) and weakly luminescent when bound to a polypyridines.<sup>23</sup>

Dichloro(*p*-cymene) ruthenium (II) dimer



In a proof-of-principle study, a solution of HPhen1 was treated with a 5-fold molar excess of compound **1** (i.e., 10-fold excess Ru) dissolved in DMSO and stirred at room temperature for  $\sim 4$  days. Reactions were quenched by removing unreacted **1** via gel filtration and subsequently purified by ion exchange chromatography. The FPLC chromatogram and corresponding mass spectra indicate that the only major product of the reaction is HPhen1 bound to a single Ru(*p*-cymene) adduct (Figure 11), with no discernible unlabeled or multiply labeled species. The absorbance spectra of the isolated Ru(*p*-cymene)–(HPhen1) complex features the expected shift to  $\sim 286$  nm in the Phn  $\pi$ – $\pi^*$  band due to metal binding as well as a new band at 326 nm (Ru(II)  $\rightarrow \pi^*$  arene MLCT) contributed by the Ru adduct (Figures S1.13 and S1.14, Supporting

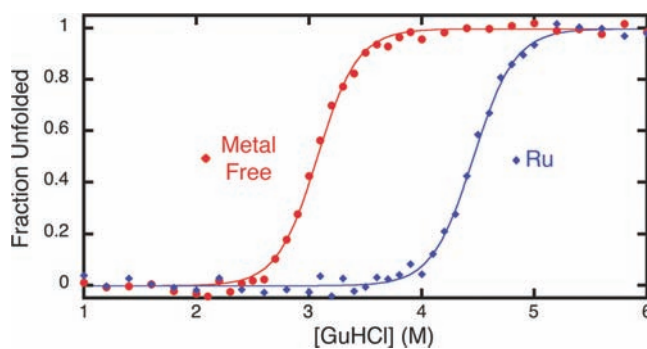


**Figure 12.** Chemical unfolding titrations (monitored by CD spectroscopy) showing the higher stability of the Ru(*p*-cymene)–HPhen1 complex (blue) with respect to HPhen1 in the absence of metals (red).

Information). When excited at 326 nm, Ru(*p*-cymene)–HPhen1 displays a weak emission band centered at 442 nm. Both the absorbance (Figure S1.14, Supporting Information) and the emission (Figure S1.15, Supporting Information) features of Ru(*p*-cymene)–HPhen1 are similar to those of an analogous model complex, [(*p*-cymene)–Ru(phen)(1-(4-cyanophenyl)imidazole)], in support of the intended mode of Ru coordination to the His–Phen HCM.<sup>23</sup>

We then examined the chemical unfolding behavior of the Ru(*p*-cymene)–HPhen1 complex to study the effects of HCM capping by a substitution-inert metal complex on protein stability. As shown in Figure 12, binding of Ru(*p*-cymene) to HPhen1 leads to a significantly larger extent of stabilization compared to substitution-labile divalent metals (Figure 6 and Table 2), with a corresponding shift in the unfolding midpoint of  $\sim 1.5$  M GuHCl. Under the reasonable assumption that Ru(*p*-cymene) is still bound to the His–Phen HCM upon denaturation (which is not necessarily the case for labile metals), the unfolding of Ru(*p*-cymene)–HPhen1 can now be treated as a two-state process, allowing the determination of the free energy of stabilization ( $\Delta\Delta G_{\text{folding}}$ ) by Ru(*p*-cymene) binding to be 4.1 kcal/mol.<sup>24</sup> The finding that global protein stability is raised to such an extent by the metal-mediated cross-linking of a local fragment is particularly significant given that the free energy of unfolding for natural proteins typically ranges from 5 to 15 kcal/mol.<sup>25</sup>

**Effects of Intervening Residues in  $i/i+7$  HCMs.** To probe if tridentate  $i/i+7$  HCMs may be used on any helical protein surface regardless of the amino acid content, we took a closer look at the structural features of our variants with particular focus on the residues that lie between the coordinating His and the functionalized Cys. Figure 13a shows the Ni coordination mode of the His–Quin HCM in the previously determined Ni:HQuin<sub>12</sub> structure, and Figure 13b shows the proposed conformation for HPhen1 modeled after the same structure. These structures clearly indicate that the only intervening residues of interest are at the  $i+3$  and  $i+4$  positions, regardless of the relative positions of His and Cys on the helix (i.e.,  $i/i+7$  or  $i/i-7$ ).

(24) For a previous study, where a Ru–polypyridyl complex was used to crosslink two loops on cytochrome *c*, see: Muheim, A.; Todd, R. J.; Casimiro, D. R.; Gray, H. B.; Arnold, F. H. *J. Am. Chem. Soc.* **1993**, *115*, 5312–5313.

(25) Alber, T. *Annu. Rev. Biochem.* **1989**, *58*, 765–798.

(23) Singh, S. K.; Trivedi, M.; Chandra, M.; Sahay, A. N.; Pandey, D. S. *Inorg. Chem.* **2004**, *43*, 8600–8608.

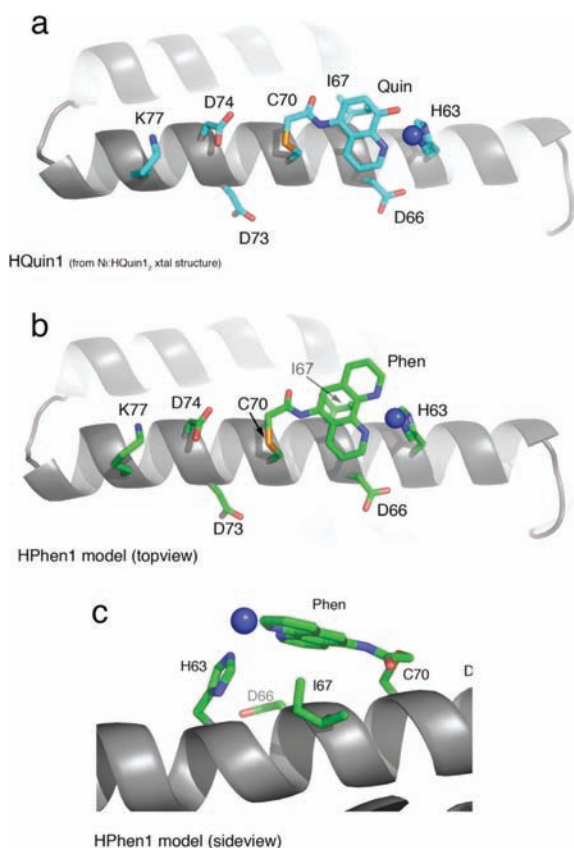


**Figure 13.** (a) Cartoon representation of the HQuin1 structure showing the Ni coordination mode by the  $i/i+7$  His–Quin HCM. Other residues on Helix3 that are important for the construction of either the HPhen3 HCM (positions 70 and 77) or those corresponding to the  $i+3$  and  $i+4$  positions for all variants are also shown as sticks. (b) The analogous representation of HPhen1 modeled after the HQuin1 structure. (c) Closeup view of the model for His–Phen HCM coordinated to  $\text{Ni}^{2+}$ .

Importantly, for both  $i+3$  and  $i+4$  positions (Asp66 and Ile67 for HPhen1 and HQuin1), the  $\text{C}_{\text{backbone}}-\text{C}_{\alpha}$  vectors that largely dictate the orientation of the side chains are directed away from the coordinating groups. It could then be expected that the  $i/i+7$  His–Phen or His–Quin HCMs may be universally installed on any regular  $\alpha$ -helical surface to coordinate metals without significant interference by the intervening amino acids. This expectation is supported by the finding that HPhen1, HPhen2, and HPhen3 display more or less similar binding affinities for several divalent metal ions (Table 1) despite different sets of intervening residues: Asp66/Ile67 for HPhen1, Ile67/Asp66 for HPhen2 (inverse of HPhen1), and Asp73/Asp74 for HPhen3 (Figure 13a and b).

At the same time, a close inspection of the HQuin1 structure and the HPhen1 model (Figure 13c) shows that the side chain of Ile67 forms van der Waals contacts ( $d \sim 3.0$  Å) with the Quin (or Phen) aromatic ring. These favorable interactions would be absent in the case of HPhen2 or HPhen3, which would respectively present Asp66 or Asp74 near the vicinity of Quin or Phen. Such differential interactions are likely culprits for the lack of any obvious trend in the metal binding affinities of HPhen1, HPhen2, and HPhen3 (Table 1). Nevertheless, we envision that the  $i+3$  and  $i+4$  positions within  $i/i+7$  HCMs may be exploited as additional handles to fine-tune metal coordination by HCMs.

## Conclusion

Cumulatively, our studies establish that  $i/i+7$  HCMs that include a single His and a non-natural bidentate ligand like Phen and Quin can form tridentate chelating platforms on  $\alpha$  helices, extending the scope of coordination chemistry on protein surfaces. Such tridentate HCMs not only provide unprecedented metal binding affinities but are also able to stabilize  $\alpha$ -helical structures, lead to the formation of discrete oligomers, and provide high-affinity attachment sites for metal-based probes. Our findings and analyses suggest that these HCMs may be utilized as modular units on any  $\alpha$ -helical protein surface in a sequence-independent fashion.

## Experimental Section

**Materials and Methods.** Unless otherwise noted, all solvents and buffers were purchased from Fisher Scientific or VWR and used without further purification. ACS reagent-grade metal salts ( $\text{CoCl}_2$ ,  $\text{NiSO}_4$ ,  $\text{CuSO}_4$ , and  $\text{ZnCl}_2$ ) were purchased from Sigma-Aldrich and used without further purification.

**Mass Spectrometry.** Protein mass spectrometry was carried out at the Biomolecular/Proteomics Mass Spectrometry Facility at UCSD using a Voyager DE-STR MALDI-TOF mass spectrometer. Protein samples (100  $\mu\text{L}$ ) were first washed three times with 400  $\mu\text{L}$  of nanopure water (Millipore) using a centrifugal spin column (Millipore) equipped with a 10 kDa cutoff filter. In a typical experiment, 5  $\mu\text{L}$  of a protein sample was mixed in a 1:1 ratio with sinapinic acid (Aligent) as a matrix. A total of 1  $\mu\text{L}$  of the resulting protein/matrix samples was plated on a standard 100 well plate and dried completely before use.

Mass spectrometry (MS) of small molecules was carried out at the Molecular Mass Spectrometry Facility at UCSD using either electrospray ionization (ESI) or an atmospheric pressure chemical ionization (APCI) source on a ThermoFinnigan LCQDE-CA mass spectrometer equipped with a quadrupole ion trap mass analyzer and Xcalibur data system. The MS detector was operated under both the positive and negative ion modes with a mass resolution range of 100 ppm.

**Site-Directed Mutagenesis.** Site-directed mutagenesis was performed on the pETc-b562 plasmid (denoted as wild-type)<sup>26</sup> using the QuikChange kit (Stratagene) and employing primers obtained from Integrated DNA Technologies. The mutant plasmids were transformed into XL-1 Blue *E. coli* cells and purified using the QIAprep Spin Miniprep kit (Qiagen). Point mutations were introduced to obtain the following *cyt cb*<sub>562</sub> variants: G70C-*cyt cb*<sub>562</sub>, G70H/H63C-*cyt cb*<sub>562</sub>, K77C/G70H/H63A/W59H-*cyt cb*<sub>562</sub>, and G70C/H63A-*cyt cb*<sub>562</sub>. Sequencing of all mutant plasmids was carried out by Retrogen Inc. (San Diego, CA).

**General Protein Expression and Purification Protocol.** The mutant plasmids isolated from XL-1 blue cells were transformed into BL21(DE3) *E. coli* cells along with the *cm* heme maturation gene cassette plasmid, pEC86.<sup>27</sup> Cells were plated on LB agar, containing 100  $\mu\text{g}/\text{mL}$  ampicillin and 34  $\mu\text{g}/\text{mL}$  chloramphenicol, and grown overnight. From these colonies, an LB medium was then inoculated and allowed to incubate for 16 h at 37 °C, with rotary shaking at 250 rpm. No induction was necessary.

Mutant-expressing cells were sonicated, brought to pH 5 with the addition of HCl, and centrifuged at 16 000 g at 4 °C for 1 h. The protein was then purified by ion-exchange chromatography on a CM-Sepharose matrix (Amersham Biosciences) using a NaCl gradient in a sodium acetate buffer (pH 5). After exchange

(26) Faraone-Mennella, J.; Tezcan, F. A.; Gray, H. B.; Winkler, J. R. *Biochemistry* **2006**, *45*, 10504–10511.

(27) Braun, M.; Thony-Meyer, L. *Proc. Natl. Acad. Sci. U.S.A.* **2004**, *101*, 12830–12835.



into a sodium phosphate buffer (pH 8) using 6–8 kDa cutoff dialysis tubing (Fisher), the protein was further purified using an Uno-Q (BioRad) anion exchange column on a DuoFlow chromatography workstation (BioRad) using a NaCl gradient. Protein purity was determined by SDS-PAGE gel electrophoresis. Verification of mutations was made through MALDI mass spectrometry (Table 3).

**Synthesis of Iodoacetic Anhydride.** As a precursor, iodoacetic acid anhydride was freshly prepared by adding 2.64 g (12.8 mmol) of DCC to a stirred solution of 5.0 g (26.8 mmol) of iodoacetic acid in 75 mL of ethyl acetate. Dicyclohexylurea precipitates immediately, but the mixture was allowed to stir for 2 h in the dark. Dicyclohexylurea was removed by filtration, and the resulting solution was evaporated to dryness and used immediately.

**Synthesis of 5-Iodoacetamido-1,10-phenanthroline (IA-Phen).** A total of 0.5 g (2.56 mmol) of 5-amino-1,10-phenanthroline (Polysciences) was dissolved in 90 mL of acetonitrile with slight heating. To this stirred solution, the freshly prepared iodoacetic acid anhydride dissolved in 10 mL of acetonitrile was added. The mixture was allowed to react in the dark overnight. The precipitated product was isolated by filtration and washed with cold 5% sodium bicarbonate, followed by water and dried in vacuo. Both the ESI MS (Figure S1.16, Supporting Information) and NMR spectra correspond to previously reported literature values<sup>22</sup> (yield: 75%).

**Synthesis of Iodoacetamido-8-hydroxyquinoline (IA-Quin).** A total of 0.5 g (2.14 mmol) of 5-amino-8-hydroxyquinoline dihydrochloride (Sigma) was dissolved in 30 mL of acetonitrile by refluxing overnight with 975  $\mu$ L (7 mmol) of triethylamine. The resulting solution was filtered, and iodoacetic acid anhydride, dissolved in 5 mL of acetonitrile, was added. The mixture was allowed to react in the dark overnight. The product evaporated to dryness and was washed extensively with cold 5% sodium bicarbonate followed by water and was dried in vacuo (yield: 75%). Synthesis of IA-Quin was verified by mass spectrometry (ESI-MS, positive mode, Figure S1.17, Supporting Information). Measured MW = 328.96  $m/z$  (exp.: 328.9) ( $M + H^+$ ).

**Synthesis of 4-Iodoacetamido-2,2':6',2''-terpyridine (IA-Terpy).** 4-Amino-2,2':6',2''-terpyridine ( $NH_2$ -Terpy) was prepared as previously described.<sup>28</sup> A total of 0.1 g (0.4 mmol) of  $NH_2$ -Terpy was dissolved in 20 mL of dry dichloromethane. To this solution was added 200  $\mu$ L (1.4 mmol) of triethylamine, and the reaction mixture was cooled to 0 °C by stirring in an ice bath. Once the temperature equilibrated (approximately 20 min), 54  $\mu$ L (0.6 mmol) of iodoacetyl chloride was added in a dropwise fashion. The mixture was left to react in the dark at 0 °C for 30 min and was then slowly brought up to room temperature. After a total period of 1 h, the reaction volume was doubled with dichloromethane and washed extensively with cold 5% sodium bicarbonate followed by water. The organic fractions were evaporated, dried in vacuo, and used without further purification (yield: ~60%). In addition to IA-Terpy, small amounts of the amino precursor and a chloroacetamide terpyridine adduct were present as impurities. However, since only IA-Terpy can efficiently modify the protein under relevant labeling conditions, the product was used without further purification. Product formation was verified by mass spectrometry (ESI-MS, positive mode, Figure S1.18, Supporting Information). Measured MW = 417.05  $m/z$  (exp.: 417.22  $m/z$ ) (IA-Terpy +  $H^+$ ); 325.29  $m/z$  (exp.: 325.08  $m/z$ ) (CIA-Terpy +  $H^+$ ); 249.44  $m/z$  (exp.: 249.11  $m/z$ ) ( $NH_2$ -Terpy +  $H^+$ ).

**General Protocol for Functionalization of cyt  $cb_{562}$  Variants with Phen and Terpy Chelates.** A solution of 0.3 mM cyt  $cb_{562}$  in

Table 3

| cyt $cb_{562}$ variant | calcd. MW (amu) | obsd. MW (amu) |
|------------------------|-----------------|----------------|
| G70C                   | 12386           | 12385          |
| H63C/G70H              | 12386           | 12386          |
| K77C/G70H/H63A/H59H    | 12280           | 12282          |
| H63A/G70C              | 12320           | 12320          |

Table 4

| Cyt $cb_{562}$ variant            | calcd. MW (amu) | obsd. MW (amu) |
|-----------------------------------|-----------------|----------------|
| G70C-Phen (HPhen1)                | 12622           | 12622          |
| G70H/H63C-Phen (HPhen2)           | 12622           | 12620          |
| W59H/H63A/G70H/K77C-Phen (HPhen3) | 12516           | 12513          |
| G70C-Quin (HQuin1)                | 12589           | 12590          |
| G70C-Terpy (HTerpy1)              | 12675           | 12680          |
| H63A/G70C-Phen (APhen1)           | 12556           | 12552          |

degassed 0.1 M Tris buffer (pH 7.75) was treated with a 10-fold excess of dithiothreitol (DTT) (Sigma). The protein was allowed to reduce for a period of 30 min. The protein was then dialyzed against  $2 \times 1$  L of degassed 0.1 M Tris buffer (pH 7.75) under an inert atmosphere to remove DTT. A 10-fold excess of the iodoacetamide label was dissolved in 2 mL of degassed DMF and added dropwise to the protein solution over the course of 1 min. The mixture was allowed to react in the dark at 25 °C overnight and then dialyzed again against  $2 \times 1$  L of 10 mM sodium phosphate buffer (pH 8) and 1 mM EDTA. The crude labeled protein was subsequently purified on an Uno-Q anion-exchange column (BioRad) using a sodium chloride gradient. If further purification was necessary, the labeled fractions were combined and dialyzed against  $2 \times 1$  L of 10 mM sodium acetate buffer (pH 5) and 1 mM EDTA. The protein mixture was then purified on an Uno-S (BioRad) cation-exchange column using a sodium chloride gradient. The final purity of the functionalized protein was determined to be greater than 95% by MALDI mass spectrometry and SDS-PAGE electrophoresis (labeling yield: 60–95%; Table 4).

**Metal Binding Titrations.** Metal ( $M^{2+}$ ) binding titrations were performed by stepwise addition of concentrated metal stock solutions to 2 mL protein stock solutions (2 to 5  $\mu$ M) prepared in 50 mM MOPS (pH 7) pretreated with Chelex resin (BioRad). All pipet tips were rinsed  $3 \times$  in an analytical grade 5%  $HNO_3$  (Fluka) solution before use. All further procedures followed to ensure a metal-free environment have been previously outlined by Linse.<sup>29</sup>

Titration data obtained by monitoring changes in the Phen/Terpy absorption were fit using nonlinear regression on Dynafit 3 (BioKin). All absorption spectra were obtained on an HP 8452A spectrophotometer. HPhen and HTerpy concentrations were determined on the basis of the Soret absorption maximum for cyt  $cb_{562}$  at 415 nm ( $\epsilon = 0.148 \mu M^{-1} cm^{-1}$ ). All data were baseline-corrected and adjusted for dilution. Due to the tendency of the HPhen and HTerpy variants to undergo metal-mediated dimerization, data were separately fit to both 1:1 and 1:1/1:2 models. The later model accounts for both metal binding and metal-mediated protein dimerization.

**Chemical Unfolding Studies.** A total of 5 mL of an unfolded protein solution containing 5  $\mu$ M of HPhen/HTerpy and 1 mM of  $M^{2+}$  or EDTA was freshly prepared in ~8 M guanidine HCl (GuHCl) in the appropriate buffer (either 100 mM Tris buffer (pH 7.5) or 100 mM sodium acetate (pH 5.5)). In parallel, 3 mL of a folded protein solution containing 5  $\mu$ M of the same variant in the appropriate buffer and 1 mM  $M^{2+}$  or EDTA was

(28) Zhou, Z. G.; Sarova, G. H.; Zhang, S.; Ou, Z. P.; Tat, F. T.; Kadish, K. M.; Echegoyen, L.; Guldi, D. M.; Schuster, D. I.; Wilson, S. R. *Chem.—Eur. J.* 2006, 12, 4241–4248.

(29) Linse, S. *Calcium-Binding Protein Protocols: Methods and Techniques*; Vogel, H. J., Ed.; Humana Press: Totowa, NJ, 2002; Vol. 2.

prepared. The unfolded protein stock was titrated into the folded protein stock at 25 °C using an autotitrator (Microlab 500 Series), keeping the sample volume constant at 2 mL. Protein unfolding was monitored by CD spectroscopy (222 nm) on an Aviv 215 spectrometer. For every titration point, the solution was allowed to stir for 30 s in order to reach equilibrium. This procedure was repeated for a minimum of 30 points covering a GuHCl range of 0.1–6.5 M. GuHCl concentrations were calculated using the refractive indices of the folded and unfolded protein stock solutions.<sup>30</sup> Unfolding data were fit using Kaleidagraph (Synergy Software) with an expression that assumes a two-state folding/unfolding equilibrium as described by Pace et al. (eq 1).<sup>31</sup>

$$\text{Fraction Unfolded} = \frac{\exp(-m1 \times (m2 - [\text{GuHCl}])/RT)}{1 + \exp(-m1 \times (m2 - [\text{GuHCl}])/RT)} \quad (1)$$

where  $m1$  represents the slope of the unfolding transition and is defined as  $(\partial\Delta G_{\text{H}_2\text{O}}/\partial[\text{GuHCl}])$ , and  $m2$  represents the midpoint GuHCl concentration where 50% of the protein is unfolded. All HPhen and HTerpy variants remain in their monomeric form under the conditions (5  $\mu\text{M}$  of protein, 1 mM  $\text{M}^{2+}$ ) used in chemical denaturation experiments.

**Thermal Denaturation.** A 3 mL solution of 5  $\mu\text{M}$  HPhen/HTerpy in 100 mM Tris buffer (pH 7.5) and 1.5 M GuHCl was prepared. Inclusion of 1.5 M GuHCl was necessary to ensure complete protein unfolding below 373 K. The protein solutions contained either 1 mM  $\text{Ni}^{2+}$  or 1 mM EDTA. The unfolding reaction was monitored over a range of 300–376 K by CD spectroscopy (222 nm). At each temperature point, the solution was allowed to stir for 30 s in order to reach equilibrium. Although the thermal unfolding of HCMs is not completely reversible, the curve was fit to a two-state model as described by John and Weeks<sup>32</sup> to obtain an apparent  $\Delta T_m^{\text{metal}}$ . Unfolding data were fit using Kaleidagraph (Synergy Software).

**Sedimentation Velocity Experiments.** All SV samples were prepared in a 20 mM Tris buffer (pH 7). Measurements were made on a Beckman XL-I Analytical Ultracentrifuge (Beckman-Coulter Instruments) using an An-60 Ti rotor at 41 000 rpm for a total of 250 scans per sample. The following wavelengths were used for detection: 418 nm (5  $\mu\text{M}$  protein), 420 nm (10  $\mu\text{M}$  protein), 425 nm (20  $\mu\text{M}$  protein), 540 nm (40  $\mu\text{M}$  protein), 545 nm (60  $\mu\text{M}$  protein), and 560 nm (100  $\mu\text{M}$  protein).

All data were processed using SEDFIT.<sup>33</sup> Buffer viscosity, buffer density, and protein partial specific volume values were calculated at 25 °C with SEDNTERP (<http://www.jphilo.mailway.com>). The partial specific volume ( $V_{\text{bar}}$ ) for each variant was calculated assuming a partial specific volume of heme of 0.82 mg/mL and 0.71 mg/mL, 0.75 mg/mL, and 0.87 mg/mL for

Phen, Quin, and Terpy, respectively. All data were processed using fixed values for buffer density ( $\rho$ ; 0.99764 g/mL) and buffer viscosity (0.0089485 poise).

**DFT Calculations.** DFT calculations were performed with the Amsterdam Density Functional (ADF) program suite,<sup>34,35</sup> version 2007.01,<sup>36</sup> on a home-built 72-CPU (1  $\times$  8 master, 8  $\times$  8 slave) Rocks 4.3 Linux cluster featuring Intel Xeon E5335 Quad-Core 2.00 GHz processors. Job control was implemented with the Sun Grid Engine v. 5.3. Crystallographic atomic coordinates were used as input where appropriate. Optimized geometries and molecular orbitals were visualized with the ADF-View graphical routine of the ADF-GUI<sup>37</sup> and the Gaussview 3 program.

In ADF program suite calculations, the triple- $\zeta$  Slater-type orbital TZ2P ADF basis set was utilized without frozen cores for all atoms. Relativistic effects were included by use of the zero-order regular approximation (ZORA).<sup>38</sup> To ensure consistency over a range of exchange/correlation profiles, the molecular geometries and energies were evaluated with both the BP86 and OLYP functionals.

In BP86 calculations, the local density approximation (LDA) of Vosko et al.<sup>39</sup> (VWN) was coupled with the generalized gradient approximation (GGA) corrections described by Becke<sup>40</sup> and Perdew and Yue<sup>41,42</sup> for electron exchange and correlation, respectively. In OLYP calculations, the parametrized ( $X = 0.67$ ) exchange-only LDA was coupled with the GGA corrections described by Handy and Cohen (OTPX)<sup>43</sup> and Lee, Yang, and Parr (LYP)<sup>44</sup> for electron exchange and correlation, respectively.

**Acknowledgment.** This work was supported by NSF (CHE-0908115, protein design, modification, unfolding studies), DOE BES (DE-FG02-10ER46677, metal binding studies), a traineeship under an NIH Heme and Blood Training Grant (T32DK007233; R.J.R.), and Beckman Young Investigator and Hellman Faculty Scholar awards (F.A.T.).

**Supporting Information Available:** Additional experimental details, figures, and tables. This material is available free of charge via the Internet at <http://pubs.acs.org>.

(34) Te Velde, G.; Bickelhaupt, F. M.; Baerends, E. J.; Fonseca Guerra, C.; van Gisbergen, S. J. A.; Snijders, J. G.; Ziegler, T. *J. Comput. Chem.* **2001**, *22*, 931–67.

(35) Guerra, C. F.; Snijders, J. G.; te Velde, G.; Baerends, E. J. *J. Theor. Chem. Acc.* **1998**, *99*, 391–403.

(36) ADF2007.01; SCM, Theoretical Chemistry, Vrije Universiteit: Amsterdam, The Netherlands. [www.scm.com](http://www.scm.com) (accessed June 2010).

(37) ADF-GUI 2007.01; SCM: Amsterdam, The Netherlands. [www.scm.com](http://www.scm.com) (accessed February 2008).

(38) van Lenthe, E.; Baerends, E. J.; Snijders, J. G. *J. Chem. Phys.* **1993**, *99*, 4597–4610.

(39) Vosko, S. H.; Wilk, L.; Nusair, M. *Can. J. Phys.* **1980**, *58*, 1200–1211.

(40) Becke, A. D. *Phys. Rev. A* **1988**, *38*, 3098–3100.

(41) Perdew, J. P.; Yue, W. *Phys. Rev. B* **1986**, *33*, 8800–8802.

(42) Perdew, J. P. *Phys. Rev. B* **1986**, *34*, 7406–7406.

(43) Handy, N. C.; Cohen, A. J. *Mol. Phys.* **2001**, *99*, 403–412.

(44) Lee, C. T.; Yang, W. T.; Parr, R. G. *Phys. Rev. B* **1988**, *37*, 785–789.

(30) Nozaki, Y. *Methods Enzymol.* **1972**, *26*, 43–50.

(31) Pace, N. C.; Shirley, B. A.; Thomson, J. A. In *Protein Structure: A Practical Approach*; Creighton, T. F., Ed.; IRL Press: Oxford, 1990; pp 311–330.

(32) John, D. M.; Weeks, K. M. *Protein Sci.* **2000**, *9*, 1416–1419.

(33) Schuck, P. *Biophys. Chem.* **2004**, *108*, 187–200.